

Gradient boosted multi-population mortality modelling with high-frequency data

Ziting Miao *

Han Li †

Yuyu Chen ‡

July 14, 2025

Abstract

High-frequency mortality data remains an understudied yet critical research area. While its analysis can reveal short-term health impacts of climate extremes and enable more timely mortality forecasts, its complex temporal structure poses significant challenges to traditional mortality models. To leverage the power of high-frequency mortality data, this paper introduces a novel integration of gradient boosting techniques into traditional stochastic mortality models under a multi-population setting. Our key innovation lies in using the Li and Lee model as the weak learner within the gradient boosting framework, replacing conventional decision trees. Empirical studies are conducted using weekly mortality data from 30 countries (Human Mortality Database, 2015–2019). The proposed methodology not only enhances model fit by accurately capturing underlying mortality trends and seasonal patterns, but also achieves superior forecast accuracy, compared to the benchmark models. We also investigate a key challenge in multi-population mortality modelling: how to select appropriate sub-populations with sufficiently similar mortality experiences. A comprehensive clustering exercise is conducted based on mortality improvement rates and seasonal strength. The results demonstrate the robustness of our proposed model, yielding stable forecast accuracy under different clustering configurations.

Keywords: Gradient boosting; Mortality forecasting; Clustering; High-frequency data; Multi-population stochastic mortality models

*Department of Economics, University of Melbourne, Australia. ✉ zitingm@student.unimelb.edu.au

†Department of Economics, University of Melbourne, Australia. ✉ han.li@unimelb.edu.au

‡Department of Economics, University of Melbourne, Australia. ✉ yuyu.chen@unimelb.edu.au

1 Introduction

Most existing research on mortality modelling uses annual data, where short-term mortality fluctuations are often overlooked. Nevertheless, modelling high-frequency data is increasingly important as it allows for capturing short-term mortality dynamics, seasonal fluctuations, and rapid responses to shocks such as epidemics or extreme weather events. While some recent studies have utilised monthly data to improve timely forecasts and support public health planning (see e.g., [Léger and Rizzi, 2024](#); [Li and Chen, 2024](#)), the modelling of weekly mortality data remains under-researched, due to limitations in data availability. More importantly, there is an urgent need for a new modelling framework specifically designed for high-frequency mortality analysis - highlighting a crucial gap in current research.

The COVID-19 pandemic has accelerated the availability and use of weekly mortality data, which is originally collected to assess the effectiveness of national containment strategies. It enables timely and precise monitoring of recent mortality dynamics, with minimal reporting delays ([Nepomuceno et al., 2022](#)). However, weekly mortality data introduce added complexity, including stronger seasonal patterns and short-term fluctuations that challenge traditional stochastic mortality models, which are designed for lower-frequency data. To address this, we propose a modelling framework specifically designed for high-frequency settings by integrating multi-population stochastic mortality models with gradient boosting techniques. This approach uncovers seasonal patterns in both shared and country-specific mortality trends, while incorporating a highly flexible structure that accommodates heterogeneous mortality experiences across countries and age groups.

The literature on mortality modelling includes numerous efforts to develop stochastic models, both for single-population contexts (see, e.g., [Osmond, 1985](#); [Lee and Carter, 1992](#); [Jacobsen et al., 2002](#); [Renshaw and Haberman, 2006](#); [Hyndman and Ullah, 2007](#)) and for multi-population settings (see, e.g., [Li and Lee, 2005](#); [Russolillo et al., 2011](#); [Hyndman et al., 2013](#); [Danesi et al., 2015](#); [Lam and Wang, 2023](#); [Dimai, 2025](#)). In this paper, we focus on multi-population mortality models for the following reasons. First, weather-related events such as heatwaves, cold spells, and regional storms typically span across national borders, affecting multiple neighbouring countries simultaneously. Accordingly, multi-population modelling allows for the effective capture of joint mortality dynamics, offering valuable insight into the influence of common shocks across interconnected populations. Second, country-specific weekly mortality rates often exhibit considerable noise and variability, which can obscure underlying trends. This issue can be addressed by extracting the common trends across populations, which helps reveal smoother seasonal patterns by “borrowing” experience across countries, thereby generating more coherent future projections. Models based on weekly mortality data require a greater level of flexibility than traditional stochastic mortality models can provide, as they must simultaneously capture age-specific seasonal patterns (e.g., the elderly are more sensitive to temperature extremes), and geographically different seasonal trends (e.g., opposing Northern and Southern Hemisphere cycles).

Gradient boosting has emerged as a powerful tool in mortality modelling due to its flexibility and superior ability to uncover hidden patterns in the data. [Deprez et al. \(2017\)](#) incorporate a wide range of individual-level features, including gender, age, year, and cohort to better assess the impact of contributing factors on mortality. Additionally, they demonstrate how regression tree boosting can help detect more patterns and facilitate cause-of-death estimates. Tree-based ensemble methods are also shown to improve both model fitting and forecast performance (see, e.g., [Levantesi and Pizzorusso, 2019](#); [Bjerre, 2022](#); [Qiao et al., 2024](#)). Traditional gradient boosting algorithms iteratively fit weak learners to residuals, gradually improving model performance until a stopping criteria is met. Common implementations include the Gradient Boosting Machine ([Friedman, 2001](#)), XGBoost ([Chen and Guestrin, 2016](#)), and LightGBM ([Ke et al., 2017](#)).

The integration of stochastic mortality models as weak learners within a gradient boosting framework, is first investigated by [Li et al. \(2025\)](#) under a single-population setting. By developing a gradient boosted Lee–Carter model, their approach effectively combines domain knowledge from classical mortality models with the improved forecast performance offered by machine learning techniques. To forecast state-level mortality rates in the US, they incorporate a penalty term by shrinking annual mortality rates according to a predefined spatial matrix that reflects the proximity of adjacent, border-sharing states. However, this dependence structure is not applicable to a more general multi-population setting, which, for instance, may involve both the Northern and Southern Hemisphere countries.

Instead of the shrinkage approach, we propose a multi-population gradient boosting framework with the Li and Lee model ([Li and Lee, 2005](#)) being the weak learner, which we refer to as the Gradient Boosted Li and Lee model, specifically designed to accommodate high-frequency mortality data. Through iterative applications of the Li and Lee model, the proposed method can capture multiple layers of trends and seasonal variations across all age groups and countries where these patterns are often under-represented in a single fitting. Final forecasts are obtained by aggregating the sequence of fitted Li and Lee models, weighted by an optimally tuned learning rate. Moreover, our proposed algorithm terminates once all underlying patterns have been captured and the residuals exhibit white-noise behaviour, subject to a predefined maximum number of iterations. Our proposed method addresses a key limitation of the gradient boosted Lee–Carter model ([Li et al., 2025](#)), which determines its stopping criteria based on the convergence between two consecutive fits. Their approach may not be suitable for high-frequency data, where residual differences diminish rapidly between iterations. In contrast, our proposed framework employs a more comprehensive training procedure that preserves informative features across iterations, thereby enhancing the capacity of our proposed model to extract meaningful and seasonal signals from high-frequency mortality data.

In multi-population mortality modelling, the grouping strategy for sub-populations plays an important role in the identification of the shared mortality trends. [Hyndman et al. \(2013\)](#) suggest grouping sub-populations based on predefined characteristics such as sex or states within a country. Departing from this conventional approach, we employ data-driven clustering techniques to identify groups of countries that exhibit similar mortality dynamics, irrespective of economic or geographic classifications. While previous studies primarily group countries based on age-specific mortality patterns (see, e.g., [Hatzopoulos and Haberman, 2013](#); [Andreopoulos et al., 2022](#); [Boonen and Chen, 2025](#)), or form groups using a combination of country and age characteristics (see, e.g., [Léger and Mazzucco, 2021](#); [Debon et al., 2024](#)), we propose to leverage seasonal trends and cyclical structures as the basis for grouping, reflecting the unique properties of high-frequency data. In particular, we highlight the contribution of using seasonal strength, which captures the magnitude of cyclical mortality patterns across populations. In addition to seasonal strength, we consider other clustering methods based on trend slopes and on combined features, enabling a comprehensive evaluation of the robustness of the proposed model across various grouping structures. This thorough design allows us to assess whether the proposed model consistently yields the most accurate predictions with different data inputs, thereby demonstrating its stability under alternative configurations.

We apply the proposed gradient boosted Li and Lee model to weekly mortality data from 30 countries, using the Short-Term Mortality Fluctuation series published by the Human Mortality Database for the period 2015 to 2019. To ensure comparability in the timing of mortality peaks and troughs, mortality rates for Southern Hemisphere countries (Australia and New Zealand) are inverted to align with the seasonal patterns of Northern Hemisphere countries. While a random walk with drift is typically used to forecast the time trend under annual data (see e.g., [Lee and Carter, 1992](#); [Giroi and King, 2007](#); [Shapovalov et al., 2019](#)), we incorporate additional Fourier regressors ([Serfling, 1963](#)) to account for seasonal cyclical patterns, on top of the time series models. The use

of sine and cosine terms allows for the joint modelling of short-term seasonal variation and long-term decline in weekly mortality rates. Empirical results demonstrate that the proposed framework outperforms existing benchmark models in terms of both model fit and forecast accuracy. Moreover, it exhibits robustness across a range of clustering selection criteria, thereby reducing the need for extensive data preprocessing or manual input adjustments.

The contribution of this paper can be summarised as follows:

- We are among the first to model and forecast high-frequency mortality rates by introducing a flexible gradient boosting framework that employs the Li and Lee model as the weak learner within a multi-population context. To harmonise seasonal patterns across hemispheres, we propose a reciprocal transformation to mortality rates in Southern Hemisphere countries. This framework not only captures the underlying short-term seasonal cycles and declining trends, but also enhances forecast accuracy.
- We conduct a comprehensive clustering-based experiment to investigate the existence of a universally optimal strategy to group countries together and to rigorously assess the robustness of our proposed model. Although certain clustering methods lead to minor improvements while others result in slight performance declines, our proposed model consistently outperforms the baseline models across all clustering methods. The robustness of our framework is further demonstrated by its superior forecast performance, with only marginal differences observed across the three clustering approaches.

The remainder of this paper is structured as follows. Section 2 describes and visualises the weekly mortality rates of 30 countries. Section 3 introduces the proposed gradient boosted Li and Lee model. In Section 4, we present and compare the fitting and forecast performance of the proposed model against baseline models. Section 5 explores three different clustering techniques to group countries with similar mortality experiences, and evaluates the forecasting results. Finally, Section 6 concludes the paper and outlines potential directions for future research.

2 Weekly mortality data

2.1 Background and description

In response to the COVID-19 pandemic, the Human Mortality Database launched the Short-Term Mortality Fluctuations (STMF) series (STMF, 2021) in May 2020, attracting growing interest in the analysis of excess mortality. Jdanov et al. (2021) develop an online tool to visualise weekly excess deaths across countries, using 2010–2019 as the reference period. Based on STMF data from 2016–2020, Islam et al. (2021) find that excess deaths in 29 high-income countries substantially exceed officially reported COVID-19 deaths, particularly among children under 15. This result is supported by Karlinsky and Kobak (2021), who underscore the need for timely and reliable mortality data to improve forecast accuracy. Kontis et al. (2020) focus on countries with populations over four million and incorporate seasonal patterns, temperature effects, long-term trends, and weekly dependencies into their model. Their findings reveal that individuals aged 65 and older account for 94% of total excess deaths, both in absolute and relative terms. Vanella et al. (2021) apply the Principal Component Analysis to mortality data from 19 European countries. They demonstrate that country-specific models often overlook shared common trends, reducing forecast accuracy. Their study underscores the importance of accounting for mortality correlations across countries, particularly given the transnational spread of pathogens. They also identify substantial cross-country variation in excess mortality, driven by differences in public health responses and demographic structures.

While much of the literature has focused on explaining pandemic-related excess mortality, this paper aims to address the broader need for long-term mortality forecasts using high-frequency data. In this paper, we collect mortality data of 30 countries from the STMF series, excluding those with populations under two million due to the frequent occurrence of zero weekly deaths. Such data sparsity introduces substantial uncertainty and can result in unstable model estimates. We extract national-level mortality rates spanning from the second week of 2015 to the final week of 2019, comprising exactly 52 weeks per year. To address the issue of zero mortality values which result in undefined logarithmic transformations, we choose to exclude the youngest age group (0–14 years old) from our analysis. Consequently, we focus on the remaining four age groups: 15–64, 65–74, 75–84, and 85+ years old.

2.2 Visualisation

The weekly mortality rates across four age groups for all 30 countries over the period 2015–2019 are presented in Appendix A. However, the seasonal patterns are not easily discernible due to the high dimensions of the data. To facilitate a clearer examination of seasonal patterns, we present weekly mortality trends for four representative countries, Australia, England and Wales, Italy, and the US, in Figure 1. A consistent seasonal pattern is observed across all countries, with each cycle spanning approximately one year. Mortality rates tend to peak during the winter and decline in the summer, reflecting the influence of climate factors. As age increases, the seasonal pattern becomes smoother and more pronounced, suggesting a stronger and more consistent relationship between weather conditions and mortality among elder individuals. This observation aligns with findings from prior research on weather-related mortality (Huang et al., 2015). Historical evidence indicates that events such as influenza outbreaks, heatwaves, and extreme cold spells have contributed to short-term fluctuations in mortality rates (Jdanov et al., 2021), and the impacts are more pronounced on individuals aged 55 and older (Li and Tang, 2022).

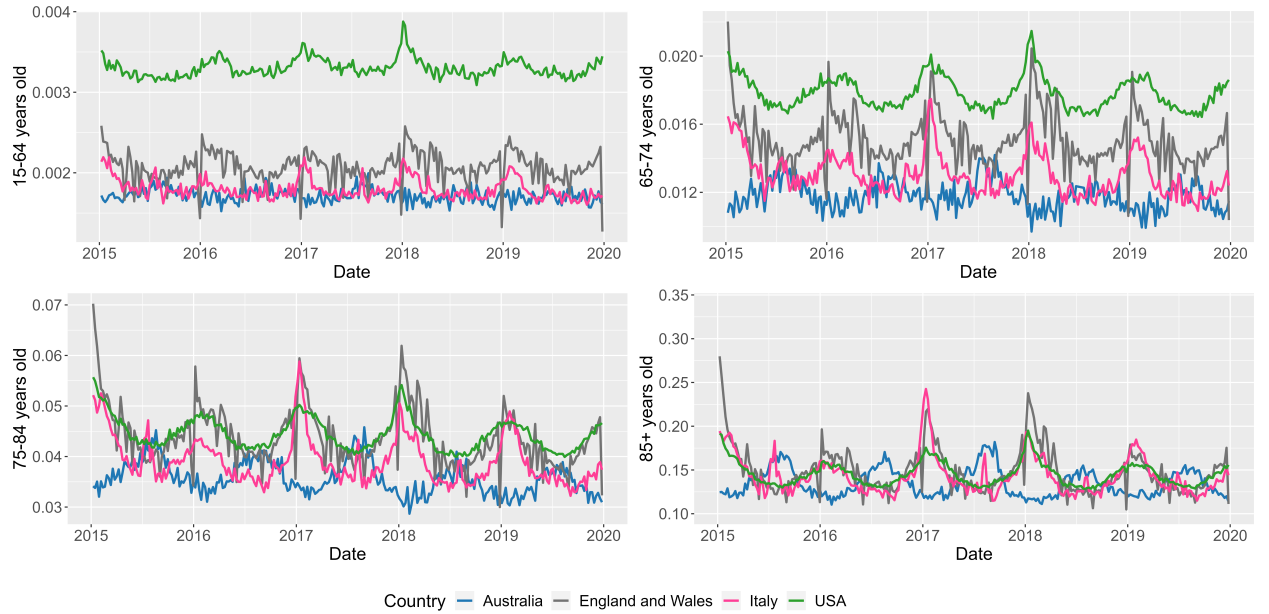


Figure 1: 2015–2019 mortality rates for the four representative countries by age groups

We then take a closer look at the seasonal timing differences between the Southern and Northern Hemispheres. In Australia, peak mortality rates occur around the middle of the year, corresponding to the winter in the Southern Hemisphere. In contrast, Italy, England and Wales, as well as the US, exhibit peak mortality at the start of the year, reflecting their winter season in the Northern Hemisphere. Notably, beyond the typical U-shaped annual mortality pattern, a W-shaped seasonal trajectory appears in certain countries during specific years. This pattern reflects two distinct mortality peaks within a year: a primary and more pronounced peak in winter, commonly associated with cold waves, and a secondary, smaller summer peak likely driven by heatwaves. The W-shaped seasonal pattern is particularly evident among elder age groups (75–84 and 85+ years old) and is especially pronounced in Italy and England and Wales.

3 Methodology

In this section, we propose a gradient boosting framework, which integrates the multi-population stochastic mortality model. Section 3.1 presents a brief description of the Li and Lee model, which serves as the weak learner within the gradient boosting framework. In Section 3.2, we outline the gradient boosting algorithm, the second key component of our methodology. Finally, Section 3.3 presents the complete formulation of the proposed Gradient Boosted Li and Lee (GBLL) model.

3.1 Li and Lee (LL) model

The Lee–Carter model (Lee and Carter, 1992) is the first single-population stochastic mortality model and serves as the foundation for the estimation of the Li and Lee model. This model separates the historical mortality rate into age-specific and time-varying components. For age group $x \in \{1, \dots, N\}$ and time $t \in \{1, \dots, T\}$, the method is formulated as follows:

$$\log(m_t(x)) = a_x + b_x \kappa_t + \varepsilon_{t,x},$$

where $m_t(x)$ is the mortality rate for age group x at time t , a_x represents the age-specific mean of log mortality rate over time, κ_t is the mortality improvement over time shared by all age groups, b_x is the corresponding age-specific loading, and $\varepsilon_{t,x}$ is an error term. The model contains two constraints to ensure the uniqueness of parameter estimates:

$$\sum_{x=1}^N b_x = 1 \quad \text{and} \quad \sum_{t=1}^T \kappa_t = 0.$$

The estimation of the Lee–Carter model is via Singular Value Decomposition (SVD), and the detailed algorithm is summarised in Appendix B. A wide range of extensions of the Lee–Carter model have been developed and published (see e.g., Brouhns et al., 2002; Cairns et al., 2006; Renshaw and Haberman, 2006; Hyndman and Ullah, 2007).

Li and Lee (2005) propose the multi-population version of the Lee–Carter model to simultaneously estimate and forecast the mortality rates of a group of populations with similar economic conditions and close-knit connections. They develop an augmented common factor model: For age group $x \in \{1, \dots, N\}$, time $t \in \{1, \dots, T\}$, and country $j \in \{1, \dots, J\}$,

$$\log(m_t^j(x)) = A_x^j + b_x^p \kappa_t^p + b_x^j \kappa_t^j + \varepsilon_{t,x}^j,$$

where A_x^j is the age-specific mean of log mortality rate over time for country j and $\varepsilon_{t,x}^j$ is the error term for country j . The common trend is captured by b_x^p and κ_t^p , obtained by applying the Lee–Carter method for the combined group including all the populations to avoid long-term divergence

in mean mortality forecasts. In addition, b_x^j and κ_t^j represent the shorter-term excessive rate of mortality change in country j over the common trend.

To estimate the Li and Lee model, we follow the product-ratio functional method proposed by Hyndman et al. (2013) with the order chosen to be 1. The detailed estimation is outlined as follows. First, let \mathbf{Y}^j denote the $T \times N$ (time \times age group) mortality matrix for country j . We then re-express the mortality rate as $m_t^j(x) = p_t(x)r_t^j(x)$ where $p_t(x)$ is the product term, calculated as the geometric mean of the mortality rate across all countries, and $r_t^j(x)$ represents the ratio term for country j (see Algorithm 1 for the definitions of $p_t(x)$ and $r_t^j(x)$). We fit separate Lee–Carter models to the product and ratio terms, to get the common factors $\hat{\kappa}_t^p, \hat{\mathbf{a}}_x^p, \hat{\mathbf{b}}_x^p$ and country-specific factors $\hat{\kappa}_t^j, \hat{\mathbf{a}}_x^j, \hat{\mathbf{b}}_x^j$, respectively. We then compute the age-specific mean as $\hat{\mathbf{A}}_x^j = \hat{\mathbf{a}}_x^p + \hat{\mathbf{a}}_x^j$. The complete estimation procedure is summarised in Algorithm 1.

Algorithm 1: Estimation of the LL Model (Product-Ratio Method)

Input: \mathbf{Y}^j for $j \in \{1, \dots, J\}$ (all with size $T \times N$)

Output: $\hat{\mathbf{y}}_x^j$ for $x \in \{1, \dots, N\}$ and $j \in \{1, \dots, J\}$

$$\hat{\kappa}_t^p = (\hat{\kappa}_1^p, \dots, \hat{\kappa}_T^p), \hat{\mathbf{a}}_x^p = (\hat{a}_1^p, \dots, \hat{a}_N^p) \text{ and } \hat{\mathbf{b}}_x^p = (\hat{b}_1^p, \dots, \hat{b}_N^p)$$

$$\hat{\kappa}_t^j = (\hat{\kappa}_1^j, \dots, \hat{\kappa}_T^j), \hat{\mathbf{a}}_x^j = (\hat{a}_1^j, \dots, \hat{a}_N^j) \text{ and } \hat{\mathbf{b}}_x^j = (\hat{b}_1^j, \dots, \hat{b}_N^j)$$

Procedure: LL(\mathbf{Y}^j)

- 1: $p_t(x) \leftarrow (m_t^1(x) \dots m_t^J(x))^{\frac{1}{J}}, \forall x, t$
 - 2: Denote \mathbf{P} by $\log(p_t(x))$ in row t and column x
 - 3: $r_t^j(x) \leftarrow \frac{m_t^j(x)}{p_t(x)}, \forall x, t$ and j
 - 4: Denote \mathbf{R}^j by $\log(r_t^j(x))$ in row t and column x
 - 5: $\hat{\kappa}_t^p, \hat{\mathbf{a}}_x^p, \hat{\mathbf{b}}_x^p \leftarrow LC(\mathbf{P}), \forall x, t$
 - 6: $\hat{\kappa}_t^j, \hat{\mathbf{a}}_x^j, \hat{\mathbf{b}}_x^j \leftarrow LC(\mathbf{R}^j), \forall x, t$ and j
 - 7: $\hat{\mathbf{A}}_x^j = \hat{\mathbf{a}}_x^p + \hat{\mathbf{a}}_x^j, \forall x, j$
 - 8: $\hat{\mathbf{y}}_{t,x}^j = \log(\hat{m}_t^j(x)) \leftarrow \hat{\mathbf{A}}_x^j + \hat{\mathbf{b}}_x^p \hat{\kappa}_t^p + \hat{\mathbf{b}}_x^j \hat{\kappa}_t^j, \forall x, t$ and j
-

3.2 Gradient boosting

Gradient boosting is an additive modelling technique that iteratively improves predictive accuracy by correcting residual errors from previous fits (Friedman, 2001). For an input matrix \mathbf{x} , the model is updated as follows. At the k -th iteration, the fitted value of the residual error $\hat{z}_k(\mathbf{x})$ is updated based on two components: the output from the previous iteration $\hat{z}_{k-1}(\mathbf{x})$, and a correction term $\lambda_k f(\mathbf{x})$, with \hat{z}_0 being the initial guess:

$$\hat{z}_k(\mathbf{x}) = \hat{z}_{k-1}(\mathbf{x}) + \lambda_k f(\mathbf{x}),$$

where λ_k is the learning rate (or shrinkage parameter) that controls the contribution of each weak learner to the final model, and $f(\mathbf{x})$ represents the weak learner, typically decision trees.

Gradient boosting, a powerful, highly flexible, and robust machine learning technique, is capable of capturing complex and non-linear relationships in data (see, e.g., [Guelman, 2012](#); [Natekin and Knoll, 2013](#); [Rushin et al., 2017](#)). This data-driven approach has gained widespread popularity across a broad range of disciplines. Its applications extend beyond the traditional domain of computer science ([Lawrence et al., 2004](#)), encompassing fields such as geology ([Zhou et al., 2016](#)), finance ([Tian et al., 2020](#)), and the insurance industry ([Su and Bai, 2020](#)).

3.3 Gradient Boosted Li and Lee (GBLL) model

Given concerns about the capacity of existing stochastic mortality models to accurately capture seasonality of mortality rates, we adopt a gradient boosting framework to iteratively model different layers of mortality trends. The Li and Lee model is employed as the weak learner to leverage domain expertise in mortality modelling, enhancing the interpretability of the overall model. Gradient boosting seeks to construct an ensemble of weak learners defined as $\mathbf{f}_x^j = \sum_{g=1}^l \gamma_g \hat{\mathbf{y}}_{x,g}^j$, where $\hat{\mathbf{y}}_{x,g}^j$ denotes the g -th prediction from the Li and Lee model for country j , γ_g represents the associated coefficient, and l is the number of iterations. This procedure involves fitting each weak learner to the residuals and solving a one-dimensional optimisation problem to determine its contribution.

To estimate the GBLL model, we first let $\mathbf{Y}^j = (\mathbf{y}_1^j, \dots, \mathbf{y}_N^j)$ denote the input mortality matrix with dimension $T \times N$ (time \times age group) for country j . In the first iteration, the parameter set $\{\hat{\kappa}_{t,1}^p, \hat{\alpha}_{x,1}^p, \hat{\beta}_{x,1}^p, \hat{\kappa}_{t,1}^j, \hat{\alpha}_{x,1}^j, \hat{\beta}_{x,1}^j\}$ is obtained by fitting the Li and Lee model to \mathbf{Y}^j . Let $\hat{\mathbf{Y}}_1^j = (\hat{\mathbf{y}}_{1,1}^j, \dots, \hat{\mathbf{y}}_{N,1}^j)$ denote the fitted value of the first iteration. The learning rate γ_1 is then determined by minimising the following quadratic loss function:

$$L_1(\gamma) = \sum_{j=1}^J \left\| \mathbf{Y}^j - \gamma \hat{\mathbf{Y}}_1^j \right\|_F^2,$$

where $\|\cdot\|_F$ represents the Frobenius norm, i.e., L_1 can be equivalently written as

$$L_1(\gamma) = \sum_{j=1}^J \sum_{x=1}^N (\mathbf{y}_x^j - \gamma \hat{\mathbf{y}}_{x,1}^j)' (\mathbf{y}_x^j - \gamma \hat{\mathbf{y}}_{x,1}^j).$$

In the $(g+1)$ -th iteration for $g \geq 1$, the parameter set $\{\hat{\kappa}_{t,g+1}^p, \hat{\alpha}_{x,g+1}^p, \hat{\beta}_{x,g+1}^p, \hat{\kappa}_{t,g+1}^j, \hat{\alpha}_{x,g+1}^j, \hat{\beta}_{x,g+1}^j\}$ and the fitted value $\hat{\mathbf{Y}}_{g+1}^j = (\hat{\mathbf{y}}_{1,g+1}^j, \dots, \hat{\mathbf{y}}_{N,g+1}^j)$ are obtained by fitting the Li and Lee model to residual \mathbf{E}_g^j from the g -th iteration, defined by:

$$\mathbf{E}_g^j = \begin{cases} \mathbf{Y}^j - \gamma_1 \hat{\mathbf{Y}}_1^j, & \text{if } g = 1, \\ \mathbf{E}_{g-1}^j - \gamma_g \hat{\mathbf{Y}}_g^j, & \text{if } g \geq 2. \end{cases}$$

Here, the learning rate γ_g for $g \geq 2$ is determined by minimising the following quadratic loss function:

$$L_g(\gamma) = \sum_{j=1}^J \left\| \mathbf{E}_{g-1}^j - \gamma \hat{\mathbf{Y}}_g^j \right\|_F^2.$$

The stopping criteria for this algorithm is when all 120 residual series, corresponding to 30 countries, each with 4 age groups, exhibit p-values of at least 0.05 under the Ljung–Box test ([Ljung and Box, 1978](#)). This indicates the absence of significant patterns in the residuals, suggesting that they behave as white-noise processes. We set the maximum number of boosting iterations to $G = 50$.

A detailed summary of this procedure is provided in Algorithm 2. The fitted log mortality rates are obtained as follows:

$$\log(\hat{m}_t^j(x)) = \sum_{g=1}^l \gamma_g \left(\hat{a}_{x,g}^p + \hat{b}_{x,g}^p \hat{\kappa}_{t,g}^p + \hat{a}_{x,g}^j + \hat{b}_{x,g}^j \hat{\kappa}_{t,g}^j \right) \text{ for all } t, x, \text{ and } j.$$

Algorithm 2: Estimation of the GBL Model

Input: \mathbf{Y}^j for $j \in \{1, \dots, J\}$ (all with size $T \times N$)

Output: $\hat{\kappa}_{t,l}^p, \hat{a}_{x,l}^p, \hat{b}_{x,l}^p$ and γ_l for $x \in \{1, \dots, N\}$, $t \in \{1, \dots, T\}$ and $l \in \{1, \dots, G\}$

$\hat{\kappa}_{t,l}^j, \hat{a}_{x,l}^j, \hat{b}_{x,l}^j$ for $x \in \{1, \dots, N\}$, $t \in \{1, \dots, T\}$, $l \in \{1, \dots, G\}$ and $j \in \{1, \dots, J\}$

Procedure: GBL(\mathbf{Y}^j)

- 1: $\hat{\mathbf{y}}_{x,1}^j, \hat{\kappa}_{t,1}^p, \hat{a}_{x,1}^p, \hat{b}_{x,1}^p, \hat{\kappa}_{t,1}^j, \hat{a}_{x,1}^j, \hat{b}_{x,1}^j \leftarrow LL(\mathbf{Y}^j), \forall x, t \text{ and } j$
 - 2: $L_1 \leftarrow \sum_{j=1}^J \sum_{x=1}^N (\mathbf{y}_x^j - \gamma \hat{\mathbf{y}}_{x,1}^j)' (\mathbf{y}_x^j - \gamma \hat{\mathbf{y}}_{x,1}^j)$
 - 3: $\gamma_1 = \arg \min_{\gamma} L_1$
 - 4: $\mathbf{e}_{x,1}^j \leftarrow \mathbf{y}_x^j - \gamma_1 \hat{\mathbf{y}}_{x,1}^j, \forall x, j$
 - 5: $\mathbf{E}_1^j \leftarrow (\mathbf{e}_{1,1}^j, \dots, \mathbf{e}_{N,1}^j), \forall j$
 - 6: $g \leftarrow 1$
 - 7: **while** $g \leq G$ **do**

$p_{x,g}^j \leftarrow \text{p-value of } \mathbf{e}_{x,g}^j \text{ under the Ljung-Box test for country } j \text{ and age group } x$
if $g = G$ **or** $\min_{x,j} p_{x,g}^j \geq 0.05$ **then**

$l \leftarrow g$
break

else

$\hat{\mathbf{y}}_{x,g+1}^j, \hat{\kappa}_{t,g+1}^p, \hat{a}_{x,g+1}^p, \hat{b}_{x,g+1}^p, \hat{\kappa}_{t,g+1}^j, \hat{a}_{x,g+1}^j, \hat{b}_{x,g+1}^j \leftarrow LL(\mathbf{E}_g^j), \forall x, t \text{ and } j$
 $L_{g+1} \leftarrow \sum_{j=1}^J \sum_{x=1}^N (\mathbf{e}_{x,g}^j - \gamma \hat{\mathbf{y}}_{x,g+1}^j)' (\mathbf{e}_{x,g}^j - \gamma \hat{\mathbf{y}}_{x,g+1}^j)$
 $\gamma_{g+1} = \arg \min_{\gamma} L_{g+1}$
 $\mathbf{e}_{x,g+1}^j \leftarrow \mathbf{e}_{x,g}^j - \gamma_{g+1} \hat{\mathbf{y}}_{x,g+1}^j, \forall x, j$
 $\mathbf{E}_{g+1}^j \leftarrow (\mathbf{e}_{1,g+1}^j, \dots, \mathbf{e}_{N,g+1}^j), \forall j$
 $g \leftarrow g + 1$
-

To ensure consistency in seasonal mortality patterns across countries, particularly between hemispheres, we apply a seasonal adjustment to Southern Hemisphere data (Australia and New Zealand) by taking the reciprocal of their mortality rates during the model estimation process. The forecasts are subsequently transformed back to the original scale, preserving interpretability while maintaining coherence within the multi-population framework.

Forecasting mortality rates primarily depends on projecting the time trend component κ_t . While traditional approaches typically use a random walk with drift, such models are often inadequate for high-frequency data with pronounced seasonal patterns. To address this, we employ a hybrid forecasting approach that combines deterministic seasonality, captured via Fourier regressors (Serfling, 1963), with a stochastic time series ARIMA(p, d, q) model. Specifically, κ_t can be modelled as follows:

$$\kappa_t = \beta_1 \sin(2\pi w(t)) + \beta_2 \cos(2\pi w(t)) + \beta_3 \sin(4\pi w(t)) + \beta_4 \cos(4\pi w(t)) + \text{ARIMA}(p, d, q),$$

where $w(t)$ represents the fractional (decimal) part of the year corresponding to the date t , and $w(t) \in [0, 1)$. There are four Fourier regressors, including both sine and cosine functions to capture both the annual and biannual cycles. If none of the Fourier components are statistically significant at the 5% level, forecasting relies solely on the ARIMA(p, d, q) model. This combined method yields the final h -step-ahead forecasts of the log mortality rate by:

$$\log(\hat{m}_{T+h}^j(x)) = \sum_{g=1}^l \gamma_g \left(\hat{a}_{x,g}^p + \hat{b}_{x,g}^p \hat{\kappa}_{T+h|T,g}^p + \hat{a}_{x,g}^j + \hat{b}_{x,g}^j \hat{\kappa}_{T+h|T,g}^j \right) \text{ for all } t, x, \text{ and } j.$$

4 Empirical results

This section evaluates both the in-sample fitting (Section 4.2) and out-of-sample forecast performance (Section 4.3) of the proposed gradient boosted Li and Lee model, in comparison with the baseline Li and Lee model (described in Section 3.1) and the Hyndman–Booth–Yasmeen (HBY) model. We first present a brief overview of the HBY model in Section 4.1.

4.1 Hyndman–Booth–Yasmeen (HBY) model

Hyndman et al. (2013) propose a generalised version of the Li and Lee model with the product-ratio functional method to forecast the mortality rate across different sub-populations coherently. The authors perform the Principal Component Analysis on both the product and ratio functions. The aggregated model for each country j is given by: For $x \in \{1, \dots, N\}$ and $t \in \{1, \dots, T\}$,

$$\log(m_t^j(x)) = \mu_j(x) + \sum_{r=1}^R \beta_{t,r} \phi_r(x) + \sum_{u=1}^U \gamma_{t,u}^j \psi_u^j(x) + z_t^j(x),$$

where $\mu_j(x)$ is the mean of log mortality rate for age group x and country j , and $\{\phi_r(x)\}$ and $\{\psi_u^j(x)\}$ are two sets of orthonormal basis functions. In addition, $\beta_{t,r}$ represents the common time trend and $\gamma_{t,u}^j$ is the country-specific time trend for $r \in \{1, \dots, R\}$ and $u \in \{1, \dots, U\}$, respectively. Finally, $z_t^j(x)$ is the error term. The HBY model can be implemented via the R package `demography`. Following Hyndman et al. (2013), we employ the HBY model with order 6 as a baseline for comparative performance evaluation. While determining the optimal order of the HBY model for high-frequency mortality data is of importance, we leave it for future investigation.

4.2 Fitting performance

We fit both the baseline models and our proposed GBLL model to mortality data from 2015 to 2018 (208 weeks). To evaluate the fitting performance of each model, we examine the behaviour of the residuals, focusing on how many countries exhibit white-noise properties within each age group. White-noise residuals indicate that the model has successfully captured all the underlying

seasonality and trends, leaving only random, patternless variations. To test this, we apply the Ljung–Box test at a significance level of 5% to determine whether the residuals can be considered white noise (Ljung and Box, 1978).

Table 1 counts the number of countries (out of 30) with white-noise residuals under each age group. We can see that for the two baseline models, the LL model performs better than the HBY model by having more countries with white-noise residuals. With more white-noise residuals, more patterns of the original data are captured, leading to a better fit and potentially improved forecast accuracy. For the HBY model, none of the 30 countries exhibit white-noise residuals for the 65–74 and 75–84 age groups. This suggests that some structures in the data remain unexplained, indicating that the HBY model is underfitting this dataset. For our proposed GBLL model, almost all countries have white-noise residuals across all the four age groups, showing its superior fitting performance by successfully extracting all insightful and predictable components. It is important to note that our comparison is limited to the HBY model with an order of 6. While alternative specifications with different orders for the HBY model may yield improved performance, exploring the full range of possible configurations is beyond the scope of this paper.

Table 1: Number of countries with white-noise residuals for each age group

Model	15–64	65–74	75–84	85+
LL	13	20	12	6
HBY	8	0	0	5
GBLL	24	27	29	26

Looking closely at those residuals that are not white noises, there remain either seasonal cyclical patterns or clear downwards/upwards sloping trends or both. This means that, given the complexity and high dimensions of the dataset, it is not suitable to use the existing methods, as they fail to capture all the patterns. For instance, in the case of Canada, residual plots from both the LL and HBY models reveal remaining seasonal cycles and trends. Figure 2 shows clear seasonal cycles for the 65–74 years old and a downwards sloping trend for the 75–84 years old, under the LL model. Similarly, Figure 3 gives the residual plot of Canada under the HBY model and there exist clear seasonal cyclical patterns for all the four age groups and a slightly decreasing trend for the 65–74 years old. Notably, the 15–64 age group exhibits an inverse seasonal pattern. This may be due to the model imposing seasonal structure to accommodate for other age groups, even though the raw data shows little seasonal variation. Additionally, the residuals for individuals aged 85 and over are approximately around ± 0.01 , clearly indicating that the HBY model struggles to capture the underlying patterns for this age group. In contrast, the residuals across all four age groups under the GBLL model exhibit white-noise behaviours, indicating improved model adequacy.

Finally, Figure 4 illustrates the contribution of each component at different stages of the model fitting process. We present the decomposition of the GBLL model for the first two iterations here, focusing on the common trends. The country-specific components breakdown are provided in Appendix C. The first column (left) displays, from top to bottom, the estimated age-specific intercepts (a_x), age loadings (b_x), and the time-varying index (κ_t) from the first iteration. The second column (right) presents the corresponding components from the second iteration.

- For the age-specific intercepts a_x , the first iteration captures a generally increasing trend. It highlights the vulnerability of elder people, resulting in higher average mortality rates. In the second iteration, a predominantly decreasing pattern is observed. Importantly, the magnitude of these adjustments is on the order of 10^{-6} , suggesting that the primary age-related mortality

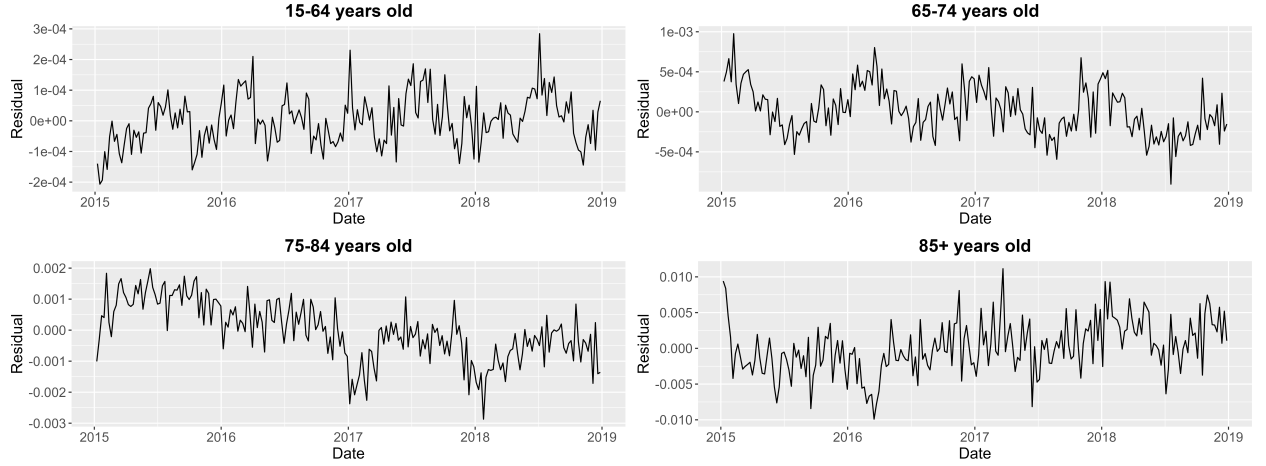


Figure 2: The residual plot of Canada under the LL model

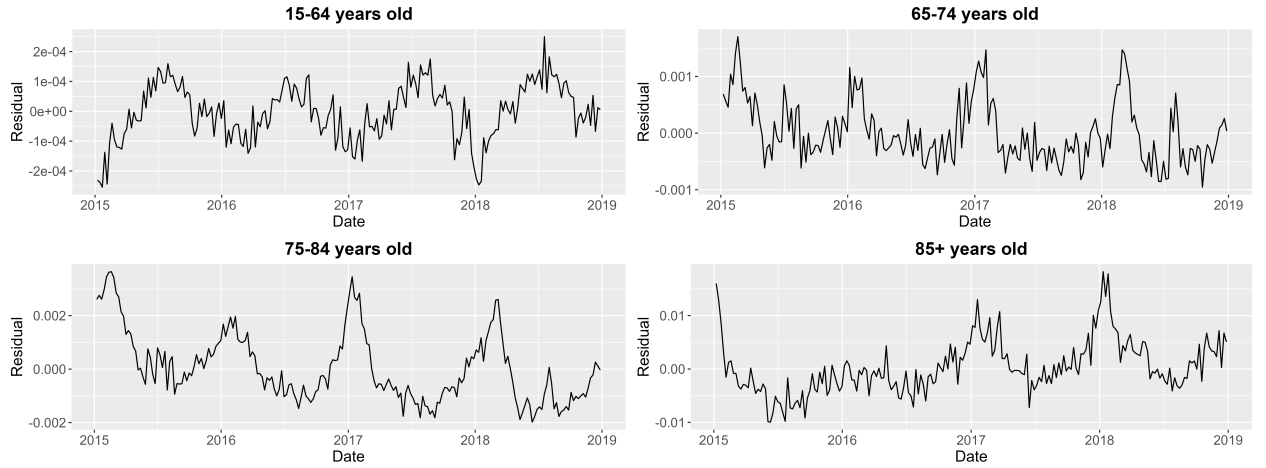


Figure 3: The residual plot of Canada under the HBY model

pattern is effectively captured in the first iteration.

- For the age loadings b_x , the first iteration exhibits an upward trend, indicating the greater exposure experienced by elder individuals to higher mortality rates. In the second iteration, a declining trend is observed. This may be related to the original smoother and more pronounced seasonal patterns typically exhibited by elder age groups. As these dominant effects are captured in the first iteration, only a small portion of the residual variation remains to be explained. Additionally, some spikes exist in the 15–64 and 85+ age groups, indicating that this iteration primarily captures residual effects concentrated in the extreme age cohorts.
- For the common time trend component κ_t , the first iteration effectively captures the dominant seasonal cycles. The second iteration provides a refinement by identifying smaller-scale cyclical patterns with short-term fluctuations and a mild downward trend, indicative of gradual improvements in mortality rates over time. A prominent W-shaped seasonal pattern is evident in the first iteration across all years, arising from the aggregation of mortality dynam-

ics across all countries. This aggregation enhances structural features that may be weakly present but commonly shared across populations, thereby making the W-shape (with dual seasonal peaks) more pronounced. Additionally, an M-shaped pattern is discernible, particularly around early 2015 and 2018. This may be attributed to the reciprocal transformation applied to the Southern Hemisphere countries, where a secondary mortality peak, likely associated with heatwaves, typically occurs at the beginning of the calendar year.

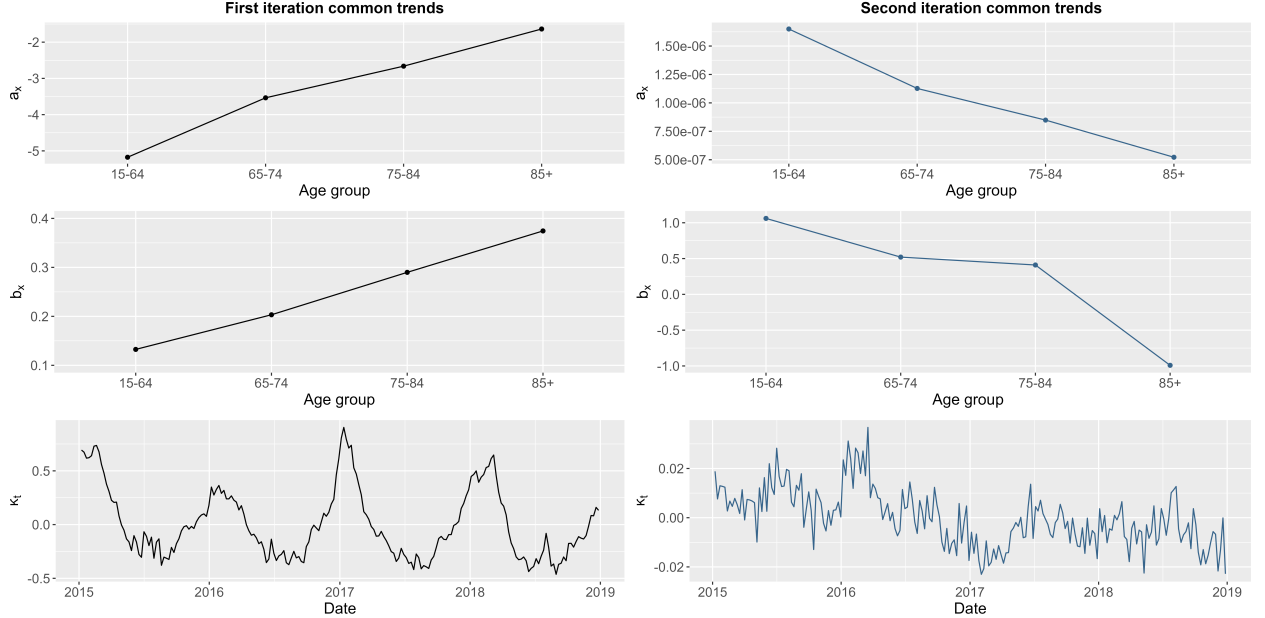


Figure 4: Components of the common trends under the GBL model: first iteration (left) and second iteration (right)

4.3 Forecast performance with expanding windows

To mitigate the impact of stochastic variability in the model fitting and forecast process, we adopt a 10-fold expanding window approach. In this setup, the starting point of the estimation window is fixed at the initial point of the dataset, the second week of January 2015. The endpoint is incrementally advanced from the final week of March 2018 to the final week of December 2018, increasing by one month at each step. This results in a progressively larger training window over successive iterations. The forecast horizon is held constant at 52 weeks, and forecast accuracy is computed monthly across all age groups and all countries. By reducing the estimation bias through repeated sampling, this approach yields more robust and reliable results.

To evaluate the forecast performance, we adopt the Mean Absolute Percentage Error (MAPE) as the error measure to quantify the average magnitude of the percentage deviation between forecasted and actual values. MAPE is scale-independent, allowing direct comparison of forecast accuracy across countries with different mortality levels. It has been widely used in the mortality forecasting literature as a standard metric for evaluating predictive performance (see e.g., [McNown and Rogers, 1992](#); [Neves et al., 2017](#); [Li et al., 2019](#); [Tsai and Cheng, 2021](#); [Qiao et al., 2024](#)). We first define the set $H = \{4, 9, 13, 17, 22, 26, 30, 35, 39, 43, 48, 52\}$, which corresponds to the cumulative number of weeks until the end of each month, thereby facilitating the conversion from weekly to

monthly forecast horizons. For month $h \in \{1, \dots, 12\}$, expanding window $r \in \{0, \dots, 9\}$, the MAPE for h -step-ahead forecasts across all age groups, countries and expanding windows is given by:

$$\text{MAPE}_h = \frac{1}{4 \times H_{(h)} \times 30 \times 10} \sum_{x=1}^4 \sum_{u=1}^{H_{(h)}} \sum_{j=1}^{30} \sum_{r=0}^9 \frac{|\hat{m}_{169+u+H_{(r)}}^j(x) - m_{169+u+H_{(r)}}^j(x)|}{m_{169+u+H_{(r)}}^j(x)},$$

where $H_{(i)}$ represents the i -th order statistic of the set H with $H_{(0)} = 0$, and 169 is the number of weeks in the first training sample.

Table 2 presents the mean MAPE of out-of-sample forecasts over the forecast horizon h from 1 to 12 months (scaled by a factor of 100). For each horizon, the lowest mean MAPE, indicating the best-performing model, is highlighted in bold. The results demonstrate that the proposed GBLL model consistently outperforms the two benchmark models across all forecast horizons. This superior performance is achieved by the iterative structure of the gradient boosting framework, which enables the model to sequentially identify and incorporate multiple layers of complex patterns.

Table 2: Mean MAPE of out-of-sample forecasts across 30 countries ($\times 100$ scale)

h	LL	HBV	GBLL
1	5.436	5.985	5.278
2	5.779	6.512	5.620
3	5.746	6.537	5.582
4	5.774	6.547	5.602
5	5.846	6.553	5.671
6	5.889	6.563	5.718
7	5.923	6.610	5.753
8	5.998	6.698	5.829
9	6.048	6.752	5.878
10	6.085	6.758	5.914
11	6.096	6.745	5.922
12	6.091	6.726	5.911

To gain a better understanding of the enhanced forecast accuracy achieved by the proposed GBLL model, Figure 5 presents the improvement in MAPE across countries and forecast horizons. Compared to the standard LL model, the GBLL model consistently enhances forecast accuracy. Substantial gains are observed in countries such as South Korea and Taiwan, while Lithuania is slightly better under the LL model. Relative to the HBV model, GBLL again shows superior performance in nearly all cases, except for Hungary in the first two forecast months. Overall, the GBLL model achieves the highest accuracy across the three models evaluated. Interestingly, the LL model outperforms the HBV model despite its simpler structure. A likely explanation is that the use of only four age groups, as opposed to single-year-of-age data for which the HBV model is designed, reduces the number of principal components needed to explain the variation in data. Consequently, the additional principal components may contribute little beyond the first. Therefore, given the complexity and heterogeneity of mortality data across 30 countries, simpler or progressive approaches such as the gradient boosting framework, may be better suited to capturing shared and country-specific patterns than more complex one-step models.

To break down the forecast performance by age groups, we present the results in Table 3. For the 15–64, 65–74, and 75–84 age groups, the proposed GBLL model consistently delivers the most accurate forecasts, outperforming both the baseline LL and HBV models. Once again, the

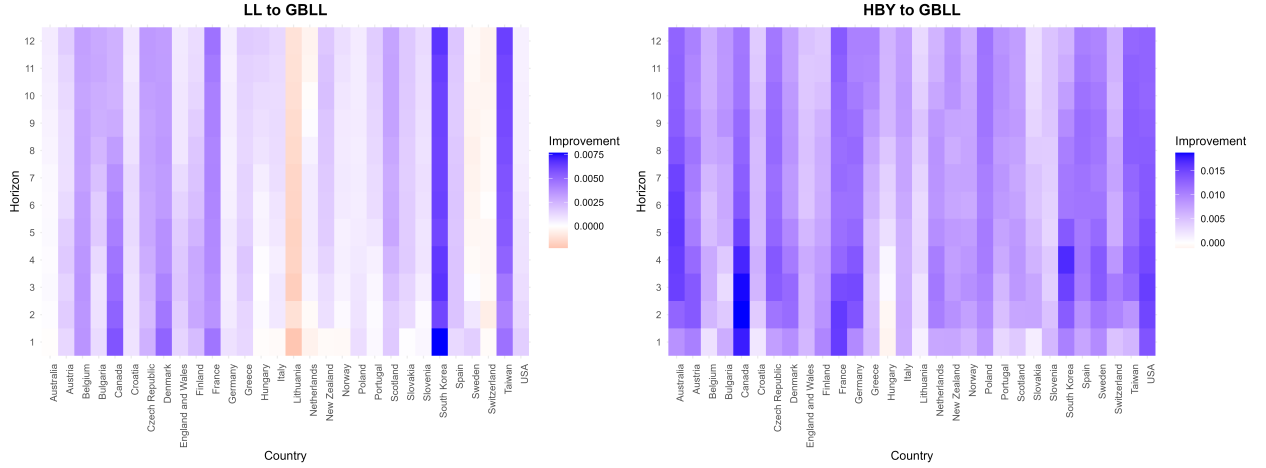


Figure 5: Improvement in MAPE from LL to GBL (left) and from HBY to GBL (right)

HBY model exhibits the weakest performance across these groups. However, for the eldest age group (85+ years old), the LL model surpasses the GBL model for 11 out of the 12 forecast horizons, with the exception of the first month. Nonetheless, the differences in MAPE between the two models are marginal. A possible explanation is that mortality patterns among the 85+ age group exhibit smoother and more dominant seasonal cycles, which are already well captured by the simpler LL model. Consequently, the LL model performs comparably or even slightly better in this case, leaving less room for improvement through the gradient boosting approach. In contrast, the three younger age groups exhibit noisier and less obvious seasonal behaviours. In these cases, the GBL model, through its iterative process, is better suited to identifying and isolating age-specific dynamics by removing residual cycles that may have been inadvertently imposed by the dominant patterns of the eldest group. As a result, the forecast performance is significantly enhanced.

Table 3: Mean MAPE of out-of-sample forecasts across 30 countries by age groups ($\times 100$ scale)

	15–64 years old			65–74 years old			75–84 years old			85+ years old		
h	LL	HBY	GBLL	LL	HBY	GBLL	LL	HBY	GBLL	LL	HBY	GBLL
1	5.625	6.067	5.345	5.524	6.131	5.353	5.166	5.996	5.020	5.429	5.746	5.395
2	5.791	6.102	5.501	5.783	6.676	5.562	5.659	6.768	5.453	5.883	6.503	5.964
3	5.754	6.040	5.468	5.769	6.805	5.498	5.674	6.756	5.439	5.787	6.547	5.922
4	5.735	6.098	5.458	5.749	6.769	5.457	5.760	6.658	5.503	5.851	6.662	5.988
5	5.779	6.234	5.501	5.769	6.687	5.460	5.876	6.593	5.602	5.959	6.699	6.122
6	5.810	6.314	5.533	5.793	6.584	5.487	5.928	6.665	5.645	6.026	6.687	6.207
7	5.848	6.372	5.570	5.811	6.571	5.506	5.955	6.802	5.672	6.079	6.695	6.265
8	5.884	6.418	5.610	5.861	6.611	5.556	6.047	6.994	5.756	6.199	6.770	6.393
9	5.909	6.454	5.644	5.896	6.633	5.593	6.118	7.115	5.817	6.269	6.806	6.460
10	5.939	6.470	5.683	5.920	6.595	5.619	6.165	7.162	5.855	6.315	6.804	6.498
11	5.973	6.501	5.720	5.917	6.534	5.621	6.173	7.185	5.856	6.322	6.760	6.491
12	6.011	6.543	5.756	5.900	6.513	5.606	6.174	7.148	5.844	6.278	6.702	6.436

5 An experiment on clustering

Clustering is an unsupervised learning technique that partitions data into distinct groups based on similarity, aiming to ensure that observations within the same cluster are more alike than those in different clusters (Rokach and Maimon, 2005). Clustering can provide alternative data groupings based on criteria such as geographic or socio-economic factors, as well as seasonal patterns, and thus can be used to assess model robustness. Evaluating model performance across these clusters helps determine how sensitive the model is to structural heterogeneity. Minimal variation in performance suggests robustness, while significant discrepancies may indicate instability of the model. Ensuring homogeneity within clusters enhances coherence in sub-population forecasts, though achieving this is more challenging in cross-country comparisons due to diverse environmental, social and political backgrounds.

Clustering techniques are increasingly employed in mortality rate modelling to enhance the interpretability and accuracy of forecasts. Hatzopoulos and Haberman (2013) aim to construct common mortality trends across multiple populations with similar mortality experiences, enabling more coherent forecasts. They apply fuzzy c-means clustering to the main time effects, which serve as a summary of mortality dynamics. Similarly, Léger and Mazzucco (2021) adopt a functional data analysis framework to mix countries and ages in the modelling process. Tsai and Cheng (2021) investigate age-specific mortality trends and propose that grouping ages with similar temporal patterns can improve forecast performance.

5.1 Set up

Clustering typically involves four key components: the data input, clustering algorithm, distance measure, and the optimal number of clusters (Yin et al., 2024). In this paper, we first extract the time trend component κ_t for each country using the Lee–Carter model. We then consider three different variations of the raw time series as the data input to investigate population similarity, while keeping the remaining three clustering components fixed.

Clustering algorithms can be broadly classified into several categories, including partitional, hierarchical, density-based, grid-based, and model-based approaches (Ghosal et al., 2020). In this study, we adopt the K-means algorithm, a representative method within the partitional clustering framework, which minimises within-cluster sum of squares through an iterative process of centroid updating and point re-assignment (Lloyd, 1982). The accompanying method to find the optimal number of clusters is the elbow method, which plots the inertia (within-cluster sum of squares) against a range of values for the number of clusters (Thorndike, 1953). Inertia is calculated as:

$$\text{Inertia} = \sum_{q=1}^Q \sum_{\mathbf{x} \in C_q} (\mathbf{x} - \boldsymbol{\mu}_q)'(\mathbf{x} - \boldsymbol{\mu}_q),$$

where Q is the total number of clusters, \mathbf{x} is an observation assigned to cluster C_q , and $\boldsymbol{\mu}_q$ is the centroid of cluster C_q . The final optimal number is identified at the “elbow” point of the curve, where the rate of decrease in inertia slows significantly, indicating diminishing returns in clustering quality with additional clusters. Finally, the distance measure used to define similarity between data points is the Euclidean distance metric. It calculates the straight-line distance between two points in an n -dimensional space.

5.1.1 Method 1: Clustering based on raw time trend series

We begin by analysing the raw time series of the country-specific κ_t as the data input. This approach identifies three distinct clusters, as detailed in Table 4. Figure 6 presents the mean value

of the time trends for each cluster. Notably, Cluster 3, which comprises only two countries from the Southern Hemisphere, exhibits seasonal patterns that are opposite to those of the other clusters. Cluster 2 consists exclusively of European countries and displays more pronounced seasonal peaks relative to Cluster 1, highlighting its higher mortality rates in winter.

Table 4: List of countries in each cluster under Method 1

Cluster	Number of countries	Country name
1	11	Canada, Denmark, England and Wales, Finland, Netherlands, Norway, Scotland, South Korea, Sweden, Taiwan, USA
2	17	Austria, Belgium, Bulgaria, Croatia, Czech Republic, France, Germany, Greece, Hungary, Italy, Lithuania, Poland, Portugal, Slovakia, Slovenia, Spain, Switzerland
3	2	Australia, New Zealand

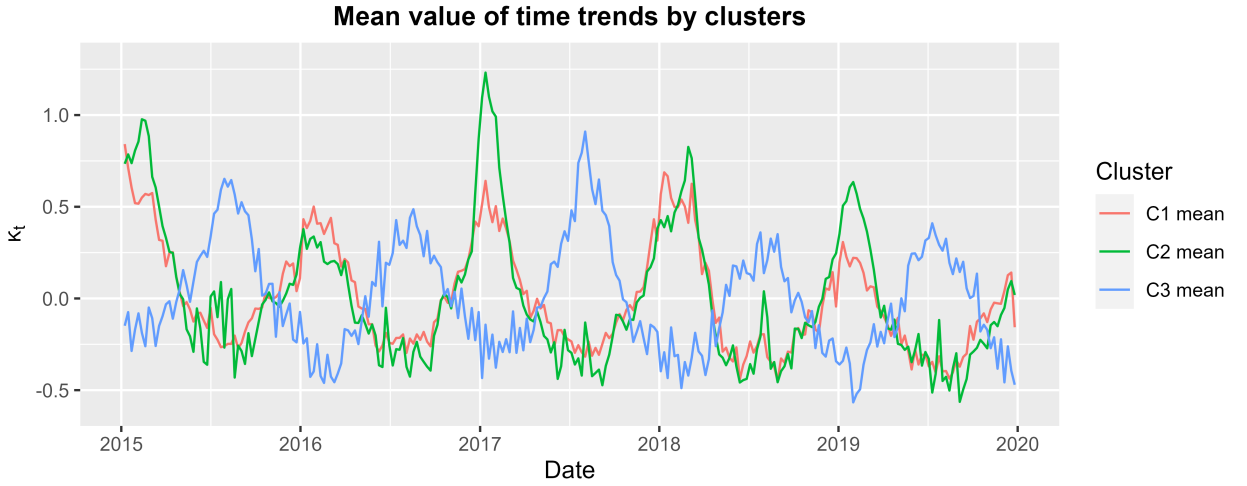


Figure 6: Mean value of the time trends in each cluster

It is noteworthy that Cluster 2 exhibits a pronounced spike during the winter of 2017, which can be attributed to an extreme cold weather event, affecting most of Europe in January. Temperatures remain significantly below seasonal averages for several days, particularly impacting southern and southeastern Europe. Greece, for instance, records its highest January mortality rate in 2017 compared to any other January between 2013 and 2018, with the elderly population aged above 80 being most affected ([Kostopoulou, 2023](#)). Italy also experiences abnormal snowfall due to cold air moving across the relatively warmer Adriatic Sea, picking up moisture and generating intense precipitation ([Murtas and Russo, 2019](#)). [Demirtaş \(2022\)](#) further investigates the broader effects of severe snowstorms and cold temperatures across southeastern Europe. A similar pattern is observed in 2019, with another cold wave, triggered by a Sudden Stratospheric Warming (SSW) event. It results in widespread snowfall and freezing temperatures across central and southern Europe, contributing to increased mortality and significant societal disruptions ([Knight et al., 2021](#)).

5.1.2 Method 2: Clustering based on estimated trend slopes

Building on the previous analysis of the raw time series, we now focus on the trend that reflects mortality improvement over years. We first apply the Seasonal and Trend decomposition using LOESS (STL) to the country-specific κ_t series (Cleveland et al., 1990). This method uses the locally estimated scatterplot smoothing (LOESS) technique to decompose each time series into three distinct components: a long-term trend, a recurring seasonal pattern, and a residual component representing irregular fluctuations. To classify countries based on their trend dynamics, we compute the slope of each decomposed long-term trend under the linear regression. This procedure identifies three distinct clusters, as detailed in Table 5. Figure 7 displays the distribution of trend slopes by clusters. Countries in Cluster 1 exhibit the most substantial mortality improvement, whereas Cluster 2 countries have moderate improvement and Cluster 3 countries are more stable over the five-year period.

Table 5: List of countries in each cluster under Method 2

Cluster	Number of countries	Country name
1	5	Croatia, Lithuania, Slovakia, South Korea, Sweden
2	12	Australia, Austria, Belgium, Czech Republic, Hungary, Italy, Norway, Scotland, Slovenia, Spain, Switzerland, Taiwan
3	13	Bulgaria, Canada, Denmark, England and Wales, Finland, France, Germany, Greece, Netherlands, New Zealand, Poland, Portugal, USA

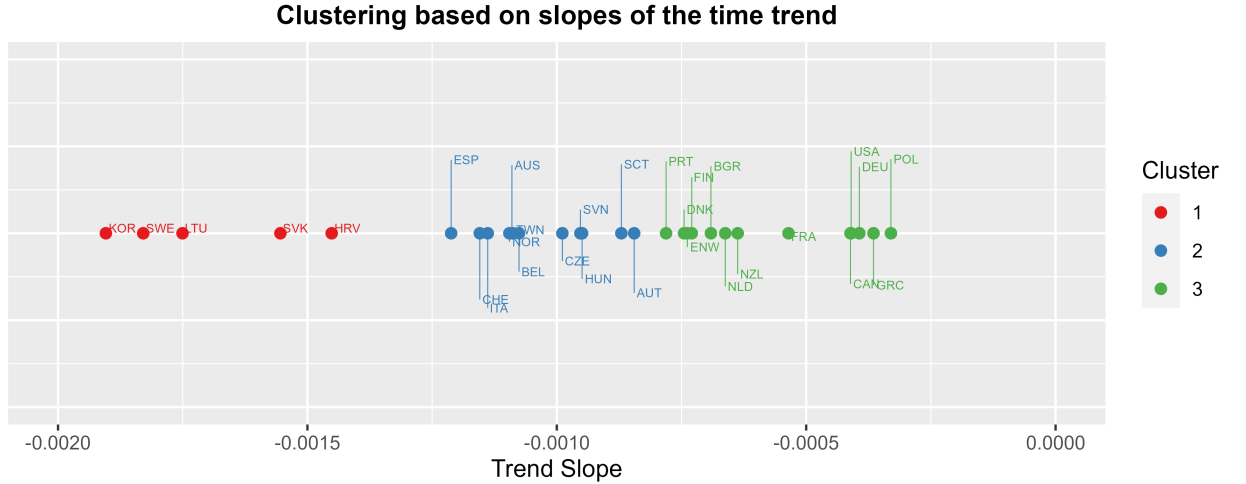


Figure 7: Trend slopes by clusters

All countries have negative trend slopes, indicating the mortality improvement across five years. The rapid mortality improvement observed in Cluster 1 may be attributed to factors such as healthcare system reforms and advances in medical technology and treatment (see, e.g., OECD, 2021; Pekarcikova, 2024). Given that countries like Croatia, Lithuania, and Slovakia have historically exhibited relatively higher mortality rates, these advancements suggest a particularly substantial improvement in health outcomes for these populations, resulting in higher trend slopes in absolute values. In Clusters 2 and 3, some geographical patterns are evident, including the group-

ing of Canada and the US, as well as several neighbouring European countries. These similarities likely reflect shared characteristics such as public health infrastructure, climatic conditions, and socio-economic contexts, which may contribute to comparable rates of mortality improvement over the period from 2015 to 2019.

5.1.3 Method 3: Clustering based on estimated trend slopes and seasonal strength

Finally, building upon the trend slopes employed in Method 2, we additionally incorporate the measure of seasonal strength derived from the aforementioned STL decomposition. These two features, trend and seasonality, are essential for characterising the underlying dynamics of mortality evolution. To ensure comparability between the two variables, min-max scaling is applied. The resulting three clusters are detailed in Table 6. Figure 8 presents a scatterplot, illustrating the clustering outcome. Cluster 1 is mainly determined by the trend slopes, where the distinction between Cluster 2 and Cluster 3 is primarily driven by differences in seasonal strength. Cluster 1 comprises countries exhibiting a higher rate of mortality improvement, as indicated by more negative trend slopes. Cluster 2 includes countries with relatively stable mortality patterns and weaker seasonality. Cluster 3 consists of countries with similar rates of mortality improvement to Cluster 2, but exhibiting stronger seasonal variations.

Table 6: List of countries in each cluster under Method 3

Cluster	Number of countries	Country name
1	5	Croatia, Lithuania, Slovakia, South Korea, Sweden
2	15	Austria, Belgium, Bulgaria, Czech Republic, Denmark, Finland, Germany, Greece, Hungary, Norway, Poland, Scotland, Slovenia, Switzerland, Taiwan
3	10	Australia, Canada, England and Wales, France, Italy, Netherlands, New Zealand, Portugal, Spain, USA

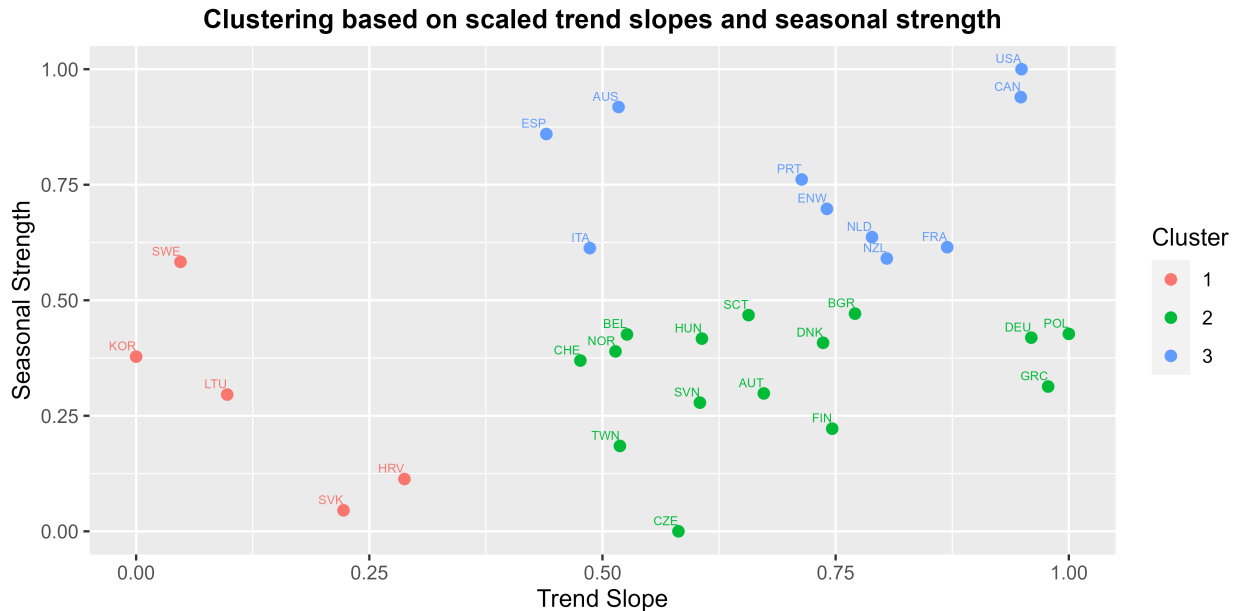


Figure 8: Clusters based on min-max scaled trend slopes and seasonal strength

We investigate the countries in Cluster 3 with respect to their pronounced seasonal mortality patterns. These stronger seasonal fluctuations are potentially attributable to cold-weather effects, which contribute to elevated mortality rates during winter months. Furthermore, all countries in Cluster 3 have aging populations, wherein elder adults exhibit increased vulnerability to seasonal health variations (Bonnet et al., 2021). Falagas et al. (2009) analyse monthly mortality data to examine seasonal patterns across Mediterranean countries, including France, Italy, Spain, and Portugal, as well as Australia, Canada, and the US. Their findings indicate that the lowest average daily mortality occurs in September for countries in the Northern Hemisphere and in March for Australia and New Zealand. These more obvious seasonal variations are further attributed to environmental factors, such as temperature and daylight duration.

5.2 Forecast performance with expanding windows

To ensure consistency in the sampling procedure, we again adopt a 10-fold expanding window approach. Table 7 summarises the forecast performance across the clustering methods described above in Section 5.1. Among the three clustering approaches, Method 1, which uses raw time trend series, yields the poorest performance, likely due to its higher dimensionality and associated noise. In contrast, Method 2, which relies solely on the slopes of country-specific time trends, achieves the best forecast accuracy. This result suggests that utilising a more distinct and parsimonious clustering criteria may facilitate the grouping of structurally similar countries, thereby enhancing predictive performance. Regardless of the clustering strategy employed, our proposed GBLL model consistently outperforms both the LL and HBY models, with the latter exhibiting the weakest forecast accuracy.

Table 7: Mean MAPE of out-of-sample forecasts across 30 countries with clustering ($\times 100$ scale)

h	Method 1			Method 2			Method 3			Whole
	LL	HBY	GBLL	LL	HBY	GBLL	LL	HBY	GBLL	GBLL
1	5.459	6.246	5.309	5.357	5.924	5.199	5.453	5.867	5.300	5.278
2	5.734	6.458	5.586	5.647	6.220	5.479	5.746	6.057	5.575	5.620
3	5.774	6.476	5.625	5.715	6.242	5.538	5.783	6.106	5.603	5.582
4	5.818	6.504	5.658	5.766	6.251	5.586	5.841	6.136	5.657	5.602
5	5.908	6.500	5.741	5.816	6.322	5.631	5.902	6.151	5.711	5.671
6	5.954	6.553	5.785	5.861	6.401	5.679	5.940	6.176	5.746	5.718
7	5.997	6.576	5.828	5.882	6.455	5.702	5.963	6.183	5.771	5.753
8	6.050	6.640	5.879	5.924	6.494	5.746	6.021	6.230	5.832	5.829
9	6.091	6.689	5.917	5.955	6.522	5.779	6.061	6.281	5.875	5.878
10	6.112	6.708	5.935	5.968	6.536	5.790	6.077	6.308	5.887	5.914
11	6.110	6.689	5.924	5.959	6.503	5.778	6.072	6.300	5.876	5.922
12	6.104	6.665	5.913	5.962	6.493	5.778	6.077	6.311	5.875	5.911

To further assess the impact of clustering, we compare the results with the case without clustering, as presented in Table 2. The overall performance remains comparable, however, Method 2 is the only clustering strategy that consistently improves forecast accuracy across all models and forecast horizons relative to the baseline case without clustering. The varying performance may be attributed to the heterogeneity in the rate of mortality improvement and the degree of seasonality across individual countries, particularly given that weekly mortality data tend to exhibit higher-frequency fluctuations and varying levels of noise. These findings suggest that, within this dataset

of 30 countries, trend slopes serve as the most effective factor for grouping countries with similar mortality experience together. Additionally, we include a reference column reporting the forecast MAPE of the GBLL model without any clustering. Notably, this unclustered version of the GBLL model still outperforms all variants of the LL and HBY models under each of the three clustering approaches and across all forecast horizons. This result highlights the robustness of the proposed GBLL framework with superior forecast performance even without clustering, surpassing baseline models that rely on clustering to enhance coherence and forecast accuracy.

Focusing on the HBY model, which emphasises the need for grouping countries with similar characteristics to enhance forecast performance, the results lend support to this premise. All three clustering methods improve forecast accuracy compared to the unclustered baseline, with the exception of the first month under Method 1. However, identifying an optimal clustering strategy that yields substantial improvement on all models over the baseline case without clustering remains challenging. This may be attributed to the limited span of data with only five years, during which there is minimal divergence in mortality trends, resulting in relatively homogeneous raw time trend series across countries. These observations underscore the importance of a modelling framework that is both adaptive and robust, regardless of clustering choices. The LL model demonstrates consistent performance across various clustering methods and may be regarded as a stable, though less flexible, approach. However, this stability comes at the cost of lower predictive accuracy. Conversely, the HBY model exhibits substantial sensitivity to country groupings and continues to deliver the weakest forecast performance overall. In contrast, the proposed GBLL model distinguishes itself by maintaining high forecast accuracy across all clustering strategies. Its performance is largely unaffected by the social, economic, or environmental heterogeneity of the countries, highlighting its robustness and superior forecasting capability.

6 Conclusion

This paper proposes a multi-population mortality model, the gradient boosted Li and Lee model that integrates gradient boosting techniques to iteratively capture the heterogeneous seasonal patterns among all age groups and countries. Specifically, we apply this model to weekly mortality rates across 30 countries for the period 2015–2019. Empirical findings demonstrate that the GBLL model outperforms the benchmark models, including the original Li and Lee model and the Hyndman–Booth–Yasmeen model of order six, in both in-sample fitting and out-of-sample forecasts. In addition, we conduct an experiment on clustering to group countries with similar mortality dynamics. Results indicate that the performance varies depending on the clustering method employed, and clustering does not universally lead to better outcomes. Nevertheless, the proposed GBLL model exhibits robustness to the choice of country groupings, maintaining stable and superior forecast accuracy across different clustering arrangements. This adaptability underscores the flexibility of the GBLL model in handling heterogeneous data without the need for extensive preprocessing or manual adjustment.

The proposed model provides several promising directions for future research. First, the reciprocal transformation of mortality rates for Southern Hemisphere countries can be leveraged in mortality risk hedging strategies, given the inverse seasonal patterns and the offset in the timing of mortality peaks and troughs across hemispheres. Second, the gradient boosting technique employed may be applied to other stochastic mortality models, such as the Cairns–Blake–Dowd model (Cairns et al., 2006) and its variants. Future research could consider finer age stratification, such as 5-year or 10-year age intervals, to provide more insights into granular dynamics and improve the precision of mortality modelling. However, this would depend on the availability of such detailed data.

Acknowledgments

The authors thank Rob J. Hyndman of Monash University, Australia, and Li Li of the University of Science & Technology Beijing, China for their helpful comments on an earlier version of this paper. Ziting Miao is supported by the Australian Government Research Training Program Scholarship and the Henry Buck Scholarship from the University of Melbourne.

Competing interest

The authors declare no conflicts of interest or competing interests in this paper.

Appendices

A Mortality data for 30 countries

While Figure A.1 does not clearly reveal country-specific mortality trends, the overarching patterns discussed in Section 2.2 remain consistent.



Figure A.1: 2015–2019 mortality rate for 30 countries by age groups

B The Lee–Carter algorithm

Following the singular value decomposition employed by Lee and Carter (1992), the estimation is conducted as follows. First let \mathbf{Y} denote a $T \times N$ (time \times age group) matrix with $\log(m_t(x))$ in row t and column x . The age-specific intercept \hat{a}_x is calculated by taking the sample mean of the logarithmic mortality rate for each age group x over T periods. Then, subtract the age-specific

intercept from each row of \mathbf{Y} and denote the resulting matrix as $\tilde{\mathbf{Y}}$. The singular value decomposition of $\tilde{\mathbf{Y}}$ gives the estimated age-specific coefficients \hat{b}_x and the estimated time component $\hat{\kappa}_t$. The completed version of the estimation procedure is summarised as follows in Algorithm B.1.

Algorithm B.1: Estimation of the Lee–Carter model

Input: \mathbf{Y} (a $T \times N$ matrix)

Output: \hat{y}_x for $x \in \{1, \dots, N\}$, $\hat{\kappa}_t = (\hat{\kappa}_1, \hat{\kappa}_2, \dots, \hat{\kappa}_T)'$, $\hat{\mathbf{a}}_x = (\hat{a}_1, \hat{a}_2, \dots, \hat{a}_N)$ and

$$\hat{\mathbf{b}}_x = (\hat{b}_1, \hat{b}_2, \dots, \hat{b}_N)$$

Procedure: LC(\mathbf{Y})

$$1: \hat{a}_x \leftarrow \frac{1}{T} \sum_{t=1}^T \log(m_t(x)), \forall x$$

$$2: \tilde{y}_{t,x} \leftarrow \log(m_t(x)) - \hat{a}_x$$

$$3: \text{Form } \tilde{\mathbf{Y}} = (\tilde{\mathbf{y}}_1, \tilde{\mathbf{y}}_2, \dots, \tilde{\mathbf{y}}_N)$$

$$4: \text{Do the Singular Value Decomposition (SVD) on } \tilde{\mathbf{Y}}$$

$$5: \hat{\kappa}_t \leftarrow d \times \mathbf{u} \times \sum_{x=1}^N v_x, \text{ where } d \text{ is the first singular value of } \tilde{\mathbf{Y}}, \mathbf{u} \text{ is the first column of the left singular vectors of } \tilde{\mathbf{Y}} \text{ and } \mathbf{v} \text{ is the first column of the right singular vectors of } \tilde{\mathbf{Y}}$$

$$6: \hat{\mathbf{b}}_x \leftarrow \frac{\mathbf{v}}{\sum_{x=1}^N v_x}, \forall x$$

$$7: \hat{y}_{t,x} = \log(\hat{m}_t(x)) \leftarrow \hat{a}_x + \hat{b}_x \hat{\kappa}_t, \forall t, x$$

C The country-specific trends under the GBLL model

In addition to the common trends discussed in Section 4.2, we present a detailed decomposition of the country-specific components under the GBLL model for the first two iterations in Figure C.1.

- For the age-specific intercepts a_x , Australia and New Zealand exhibit an opposite pattern relative to the Northern Hemisphere countries. This is due to the use of the reciprocal transformation of mortality rates. As with the common components, the primary effects are largely captured in the first iteration, as evidenced by the larger magnitudes.
- For the age loadings b_x in the first iteration, Slovenia displays elevated mortality sensitivity among individuals aged 65–74. Denmark shows comparatively higher exposure in the 15–64 age group, despite having relatively favourable outcomes for the 65–74 cohort compared to most other countries. Additionally, higher exposure is observed across all age groups except for those aged 85 and above in Netherlands. In the second iteration, the country-specific components reveal particularly pronounced deviations for Belgium and Finland, suggesting substantial excess loadings relative to other countries.
- For the time-varying index κ_t , the clear W-shaped seasonal pattern evident in the common trend is often obscured at the individual country level, largely due to local noise and country-specific variability. The first iteration captures the majority of temporal dynamics, as indicated by the larger magnitudes of the components and a lower degree of white-noise behaviour relative to the second iteration. Nonetheless, several countries exhibit unexpected

behaviours for the second iteration. For example, Denmark shows a sharp downward spike in January 2017, while Netherlands experiences a pronounced upward spike in March 2018.

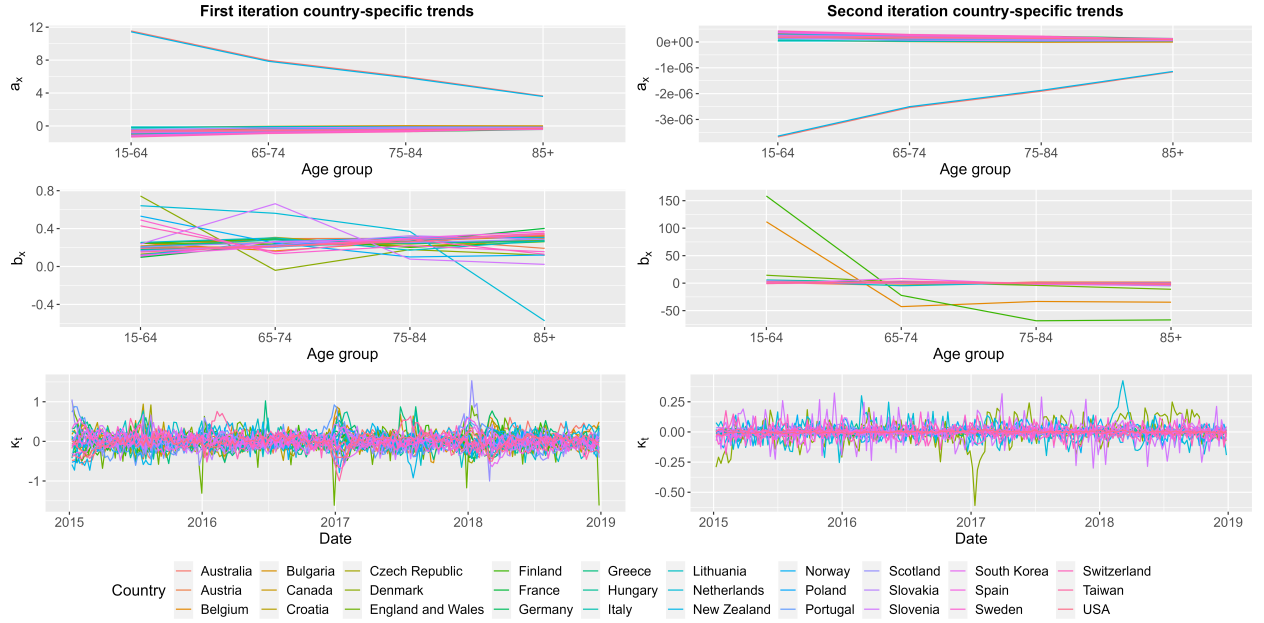


Figure C.1: Components of the country-specific trends under the GBLL model: first iteration (left) and second iteration (right)

References

- Andreopoulos, P., Bersimis, F. G., and Tragaki, A. (2022). A different approach to current developments in the twenty-first century—grouping european countries in terms of mortality. In *Quantitative Methods in Demography: Methods and Related Applications in the Covid-19 Era*, pages 373–385. Springer.
- Bjerre, D. S. (2022). Tree-based machine learning methods for modeling and forecasting mortality. *ASTIN Bulletin: The Journal of the IAA*, **52**(3):765–787.
- Bonnet, C., Cambois, E., Fontaine, R., Dutreuilh, C., and van Hoorn Alkema, B. (2021). Population ageing in high-longevity countries: demographic dynamics and socio-economic challenges. *Population*, **76**(2):217–310.
- Boonen, T. J. and Chen, Y. (2025). Low-rank tensor autoregressive models for mortality modeling. *Available at SSRN 5233127*.
- Brouhns, N., Denuit, M., and Vermunt, J. K. (2002). A poisson log-bilinear regression approach to the construction of projected lifetables. *Insurance: Mathematics and Economics*, **31**(3):373–393.
- Cairns, A. J., Blake, D., and Dowd, K. (2006). A two-factor model for stochastic mortality with parameter uncertainty: theory and calibration. *Journal of Risk and Insurance*, **73**(4):687–718.
- Chen, T. and Guestrin, C. (2016). Xgboost: A scalable tree boosting system. In *Proceedings of the 22nd ACM SIGKDD International Conference on Knowledge Discovery and Data Mining*, pages 785–794.

- Cleveland, R. B., Cleveland, W. S., McRae, J. E., Terpenning, I., et al. (1990). STL: A seasonal-trend decomposition. *Journal of Official Statistics*, **6**(1):3–73.
- Danesi, I. L., Haberman, S., and Millossovich, P. (2015). Forecasting mortality in subpopulations using Lee–Carter type models: A comparison. *Insurance: Mathematics and Economics*, **62**, 151–161.
- Debon, A., Haberman, S., and Piscopo, G. (2024). Multipopulation mortality analysis: bringing out the unobservable with latent clustering. *Quality & Quantity*, **58**(6):5107–5123.
- Demirtaş, M. (2022). The anomalously cold January 2017 in the south-eastern europe in a warming climate. *International Journal of Climatology*, **42**(11):6018–6026.
- Deprez, P., Shevchenko, P. V., and Wüthrich, M. V. (2017). Machine learning techniques for mortality modeling. *European Actuarial Journal*, **7**, 337–352.
- Dimai, M. (2025). Multi-population mortality modeling with economic, environmental and lifestyle variables. *Quality & Quantity*, **59**, 153–205.
- Falagas, M. E., Karageorgopoulos, D. E., Moraitis, L. I., Vouloumanou, E. K., Roussos, N., Pappas, G., and Rafailidis, P. I. (2009). Seasonality of mortality: the September phenomenon in Mediterranean countries. *Canadian Medical Association Journal*, **181**(8):484–486.
- Friedman, J. H. (2001). Greedy function approximation: a gradient boosting machine. *Annals of Statistics*, **29**(5):1189–1232.
- Ghosal, A., Nandy, A., Das, A. K., Goswami, S., and Panday, M. (2020). A short review on different clustering techniques and their applications. *Emerging Technology in Modelling and Graphics: Proceedings of IEM Graph 2018*, pages 69–83.
- Girosi, F. and King, G. (2007). Understanding the Lee–Carter mortality forecasting method. *Technical report, RAND Corporation*.
- Guelman, L. (2012). Gradient boosting trees for auto insurance loss cost modeling and prediction. *Expert Systems with Applications*, **39**(3):3659–3667.
- Hatzopoulos, P. and Haberman, S. (2013). Common mortality modeling and coherent forecasts. An empirical analysis of worldwide mortality data. *Insurance: Mathematics and Economics*, **52**(2):320–337.
- Huang, C., Chu, C., Wang, X., and Barnett, A. G. (2015). Unusually cold and dry winters increase mortality in Australia. *Environmental Research*, **136**, 1–7.
- Hyndman, R. J., Booth, H., and Yasmeeen, F. (2013). Coherent mortality forecasting: the product-ratio method with functional time series models. *Demography*, **50**(1):261–283.
- Hyndman, R. J. and Ullah, M. S. (2007). Robust forecasting of mortality and fertility rates: A functional data approach. *Computational Statistics & Data Analysis*, **51**(10):4942–4956.
- Islam, N., Shkolnikov, V. M., Acosta, R. J., Klimkin, I., Kawachi, I., Irizarry, R. A., Alicandro, G., Khunti, K., Yates, T., Jdanov, D. A., et al. (2021). Excess deaths associated with covid-19 pandemic in 2020: age and sex disaggregated time series analysis in 29 high income countries. *BMJ*, **373**:n1137.
- Jacobsen, R., Keiding, N., and Lynge, E. (2002). Long term mortality trends behind low life expectancy of danish women. *Journal of Epidemiology & Community Health*, **56**(3):205–208.
- Jdanov, D. A., Galarza, A. A., Shkolnikov, V. M., Jasilionis, D., Németh, L., Leon, D. A., Boe, C., and Barbieri, M. (2021). The short-term mortality fluctuation data series, monitoring mortality shocks across time and space. *Scientific Data*, **8**(1):235.
- Karlinsky, A. and Kobak, D. (2021). The world mortality dataset: Tracking excess mortality across countries during the covid-19 pandemic. *eLife*, **10**:e69336.
- Ke, G., Meng, Q., Finley, T., Wang, T., Chen, W., Ma, W., Ye, Q., and Liu, T. (2017). Lightgbm: A highly efficient gradient boosting decision tree. *Proceedings of the 31st International Conference*

- on *Neural Information Processing Systems*, pages 3149–3157.
- Knight, J., Scaife, A., Bett, P. E., Collier, T., Dunstone, N., Gordon, M., Hardiman, S., Hermanson, L., Ineson, S., Kay, G., et al. (2021). Predictability of european winters 2017/2018 and 2018/2019: Contrasting influences from the tropics and stratosphere. *Atmospheric Science Letters*, **22**(1):e1009.
- Kontis, V., Bennett, J. E., Rashid, T., Parks, R. M., Pearson-Stuttard, J., Guillot, M., Asaria, P., Zhou, B., Battaglini, M., Corsetti, G., et al. (2020). Magnitude, demographics and dynamics of the effect of the first wave of the covid-19 pandemic on all-cause mortality in 21 industrialized countries. *Nature Medicine*, **26**(12):1919–1928.
- Kostopoulou, E. (2023). Analysis of the January 2017 cold spell in greece and its implications on human health. *Environmental Sciences Proceedings*, **26**(1):195.
- Lam, K. K. and Wang, B. (2023). Multipopulation mortality modelling and forecasting: the weighted multivariate functional principal component approaches. *Journal of Applied Statistics*, **50**(15):3177–3198.
- Lawrence, R., Bunn, A., Powell, S., and Zambon, M. (2004). Classification of remotely sensed imagery using stochastic gradient boosting as a refinement of classification tree analysis. *Remote Sensing of Environment*, **90**(3):331–336.
- Lee, R. D. and Carter, L. R. (1992). Modeling and forecasting U.S. mortality. *Journal of the American Statistical Association*, **87**(419):659–671.
- Léger, A. E. and Mazzucco, S. (2021). What can we learn from the functional clustering of mortality data? An application to the human mortality database. *European Journal of Population*, **37**, 769–798.
- Léger, A. E. and Rizzi, S. (2024). Month-to-month all-cause mortality forecasting: a method allowing for changes in seasonal patterns. *American Journal of Epidemiology*, **193**(6):898–907.
- Levantesi, S. and Pizzorusso, V. (2019). Application of machine learning to mortality modeling and forecasting. *Risks*, **7**(1):26.
- Li, H. and Chen, H. (2024). Hierarchical mortality forecasting with EVT tails: An application to solvency capital requirement. *International Journal of Forecasting*, **40**(2):549–563.
- Li, H., Li, H., Lu, Y., and Panagiotelis, A. (2019). A forecast reconciliation approach to cause-of-death mortality modeling. *Insurance: Mathematics and Economics*, **86**, 122–133.
- Li, H. and Tang, Q. (2022). Joint extremes in temperature and mortality: A bivariate POT approach. *North American Actuarial Journal*, **26**(1):43–63.
- Li, L., Li, H., and Panagiotelis, A. (2025). Boosting domain-specific models with shrinkage: an application in mortality forecasting. *International Journal of Forecasting*, **41**(1):191–207.
- Li, N. and Lee, R. (2005). Coherent mortality forecasts for a group of populations: An extension of the Lee–Carter method. *Demography*, **42**, 575–594.
- Ljung, G. M. and Box, G. E. (1978). On a measure of lack of fit in time series models. *Biometrika*, **65**(2):297–303.
- Lloyd, S. (1982). Least squares quantization in PCM. *IEEE Transactions on Information Theory*, **28**(2):129–137.
- McNown, R. and Rogers, A. (1992). Forecasting cause-specific mortality using time series methods. *International Journal of Forecasting*, **8**(3):413–432.
- Murtas, R. and Russo, A. G. (2019). Effects of pollution, low temperature and influenza syndrome on the excess mortality risk in winter 2016–2017. *BMC Public Health*, **19**, 1–9.
- Natekin, A. and Knoll, A. (2013). Gradient boosting machines, a tutorial. *Frontiers in Neuro-robotics*, **7**:21.
- Nepomuceno, M. R., Klimkin, I., Jdanov, D. A., Alustiza-Galarza, A., and Shkolnikov, V. M.

- (2022). Sensitivity analysis of excess mortality due to the covid-19 pandemic. *Population and Development Review*, **48**(2):279–302.
- Neves, C., Fernandes, C., and Hoeltgebaum, H. (2017). Five different distributions for the Lee–Carter model of mortality forecasting: A comparison using GAS models. *Insurance: Mathematics and Economics*, **75**, 48–57.
- OECD (2021). *State of Health in the EU Croatia: Country Health Profile 2021*. OECD Publishing.
- Osmond, C. (1985). Using age, period and cohort models to estimate future mortality rates. *International Journal of Epidemiology*, **14**(1):124–129.
- Pekarcikova, J. (2024). Cancer mortality attributable to air pollution in slovakia. *European Journal of Public Health*, **34**(Supplement_3):ckae144.1429.
- Qiao, Y., Wang, C., and Zhu, W. (2024). Machine learning in long-term mortality forecasting. *The Geneva Papers on Risk and Insurance – Issues and Practice*, **49**(2):340–362.
- Renshaw, A. E. and Haberman, S. (2006). A cohort-based extension to the Lee–Carter model for mortality reduction factors. *Insurance: Mathematics and Economics*, **38**(3):556–570.
- Rokach, L. and Maimon, O. (2005). Clustering methods. *Data Mining and Knowledge Discovery Handbook*, pages 321–352.
- Rushin, G., Stancil, C., Sun, M., Adams, S., and Beling, P. (2017). Horse race analysis in credit card fraud—deep learning, logistic regression, and gradient boosted tree. In *2017 Systems and Information Engineering Design Symposium (SIEDS)*, pages 117–121. IEEE.
- Russolillo, M., Giordano, G., and Haberman, S. (2011). Extending the Lee–Carter model: a three-way decomposition. *Scandinavian Actuarial Journal*, **2011**(2):96–117.
- Serfling, R. E. (1963). Methods for current statistical analysis of excess pneumonia-influenza deaths. *Public Health Reports*, **78**(6):494.
- Shapovalov, V., Landsman, Z., and Makov, U. (2019). Bayesian log-bilinear mortality projection with a random walk with drift. *Available at SSRN 3375920*.
- STMF (2021). Short-Term Mortality Fluctuation Data Series. Human Mortality Database. <https://www.mortality.org/Data/STMF>.
- Su, X. and Bai, M. (2020). Stochastic gradient boosting frequency-severity model of insurance claims. *PLOS ONE*, **15**(8):e0238000.
- Thorndike, R. L. (1953). Who belongs in the family? *Psychometrika*, **18**(4):267–276.
- Tian, Z., Xiao, J., Feng, H., and Wei, Y. (2020). Credit risk assessment based on gradient boosting decision tree. *Procedia Computer Science*, **174**, 150–160.
- Tsai, C. C.-L. and Cheng, E. S. (2021). Incorporating statistical clustering methods into mortality models to improve forecasting performances. *Insurance: Mathematics and Economics*, **99**, 42–62.
- Vanella, P., Basellini, U., and Lange, B. (2021). Assessing excess mortality in times of pandemics based on principal component analysis of weekly mortality data—the case of covid-19. *Genus*, **77**, 1–36.
- Yin, H., Aryani, A., Petrie, S., Nambissan, A., Astudillo, A., and Cao, S. (2024). A rapid review of clustering algorithms. *arXiv preprint arXiv:2401.07389*.
- Zhou, J., Shi, X., Huang, R., Qiu, X., and Chen, C. (2016). Feasibility of stochastic gradient boosting approach for predicting rockburst damage in burst-prone mines. *Transactions of Nonferrous Metals Society of China*, **26**(7):1938–1945.